ISSN 0208-7774 TRIBOLOGIA 4/2019 p. 63–71
DOI: 10.5604/01.3001.0013.5966

**Aneta NIEMIEC[*], Monika MICHALAK[**], Leszek ŁATKA[***], Paweł SOKOŁOWSKI[****]**

# A COMPARISON OF TRIBOLOGICAL PERFORMANCES OF $Al_2O_3$ AND $Al_2O_3$ + 40 WT.% $TiO_2$ COATINGS MANUFACTURED BY ATMOSPHERIC PLASMA SPRAYING

# PORÓWNANIE WŁAŚCIWOŚCI TRIBOLOGICZNYCH POWŁOK $Al_2O_3$ ORAZ $Al_2O_3$ + 40% WAG. $TiO_2$ WYTWORZONYCH METODĄ ATMOSFERYCZNEGO NATRYSKIWANIA PLAZMOWEGO

**Key words:** plasma spraying, coating, microstructure, wear resistance, microhardness.

**Abstract:** In this paper, the results of tribological, microscopic and mechanical research of $Al_2O_3$ and $Al_2O_3$ + 40 wt.% $TiO_2$ coatings manufactured by atmospheric plasma spraying (APS) were presented. The feedstock materials were $Al_2O_3$ (Metco 6103, Oerlikon Metco) and $Al_2O_3$ + 40 wt.% $TiO_2$ (Metco 131VF, Oerlikon Metco) powders with the average grain size of 30 μm. The stainless steel (X5CrNi18-10) coupons had a diameter equal to 25 mm and 2 mm of thickness. The morphology and microstructure of obtained coatings were tested by scanning electron microscope (SEM). Then adhesion tests and tribological examinations by ball-on-disc (BoD) mode in technical dry friction conditions were carried out. During BoD testing, the load of 5 N was used. It was concluded that the $Al_2O_3$ coating was characterized by higher wear resistance and microhardness, but, at the same time, it was of lower fracture toughness than the $Al_2O_3$ + 40 wt.% $TiO_2$ coating.

**Słowa kluczowe:** natryskiwanie plazmowe, powłoka, mikrostruktura, odporność na zużycie ścierne, mikrotwardość.

**Streszczenie:** W artykule przedstawiono wyniki badań tribologicznych, mikroskopowych oraz mechanicznych powłok $Al_2O_3$ oraz $Al_2O_3$ + 40% wag. $TiO_2$, natryskanych metodą atmosferycznego natryskiwania cieplnego (APS). Materiałem na powłoki były proszki $Al_2O_3$ (Metco 6103, Oerlikon Metco) oraz $Al_2O_3$ + 40% wag. $TiO_2$ (Metco 131VF, Oerlikon Metco) o średniej wielkości cząstek wynoszącej 30 μm. Jako podłoże zostały użyte krążki ze stali austenitycznej X5CrNi18-10 o średnicy 25 mm i grubości 2 mm. Morfologię i mikrostrukturę uzyskanych powłok oceniono przy pomocy skaningowego mikroskopu elektronowego (SEM). Po określeniu przyczepności powłok wykonano badania tribologiczne w styku kula–tarcza w warunkach tarcia technicznie suchego. Zastosowano obciążenie 5 N. Na podstawie przeprowadzonych badań stwierdzono, że powłoki na bazie $Al_2O_3$ wykazują większą odporność na zużycie ścierne oraz wyższą mikrotwardość, ale jednocześnie mniejszą odporność na kruche pękanie ($K_{IC}$) w porównaniu z powłokami na bazie $Al_2O_3$ + 40% wag. $TiO_2$.

## INTRODUCTION

Thermally sprayed coatings have been used for more than 50 years in a wide variety of tribological, mechanical, electrical, corrosive and high-temperature applications **[L. 1]**. Thermal spraying is now regarded as a key environmentally friendly technique that modify the surface properties **[L. 2]**. Its global market (revenue from materials, equipment and coatings manufacturing) was assessed at USD 7.58 billion in 2015 and is expected to reach USD 11.89 billion by 2021 **[L. 2**, **3]**.

[*] ORCID: 0000-0001-8682-143X. Wrocław University of Science and Technology, Department of Fundamentals of Machines Construction and Tribology, 7-9 Łukasiewicza St., 50-371 Wrocław, Poland, e-mail: aneta.niemiec@pwr.edu.pl.
[**] ORCID: 0000-0003-2185-311X. Wrocław University of Science and Technology, Department of Materials Science, Strength and Welding, 7-9 Łukasiewicza St., 50-371 Wrocław, Poland, e-mail: monika.michalak@pwr.edu.pl.
[***] ORCID: 0000-0002-5236-5349. Wrocław University of Science and Technology, Department of Materials Science, Strength and Welding, 7-9 Łukasiewicza St., 50-371 Wrocław, Poland, e-mail: leszek.latka@pwr.edu.pl.
[****] ORCID: 0000-0003-2425-2643. Wrocław University of Science and Technology, Department of Materials Science, Strength and Welding, 7-9 Łukasiewicza St., 50-371 Wrocław, Poland, e-mail: pawel.sokolowski@pwr.edu.pl.

Nowadays, much attention is paid to the complex deposits, derived from powders, which compose from different metals, hardmetals, and/or oxides **[L. 4–6]**. One of intensively studied ones are $Al_2O_3$ and $Al_2O_3$ + $TiO_2$ powders, which are most commonly sprayed by the method of Atmospheric Plasma Spraying (APS) **[L. 7**, **8]**. $Al_2O_3$ is used for dense coatings in applications where good tribological properties as well as temperature- and chemical- resistance are required **[L. 9]**. The addition of $TiO_2$ to $Al_2O_3$ results in a decrease in melting temperature and gives possibilities to manufacture coatings with higher fracture toughness than in the case of pure $Al_2O_3$ **[L. 10]**. Moreover, such powders, combined from two oxides ($Al_2O_3$ and $TiO_2$) in one particle, are of better properties than each of them separately **[L. 5]**. Due to their combination of wear-, oxidation- and aggressive environments- resistance, possible applications are still increasing **[L. 11**, **12]**.

The coatings' microstructure, and mechanical and tribological properties, are strongly dependent on many factors, including both used materials and process parameters. In this paper, coatings of $Al_2O_3$ and $Al_2O_3$ + 40 wt. $TiO_2$ were sprayed by APS. Optimal parameters of the process were selected to obtain coatings with good adhesion, high fracture toughness resistance, and low porosity. Coatings were then tested for their wear resistance. The goal was to determine the effect of $TiO_2$ addition in the reference to the coatings properties.

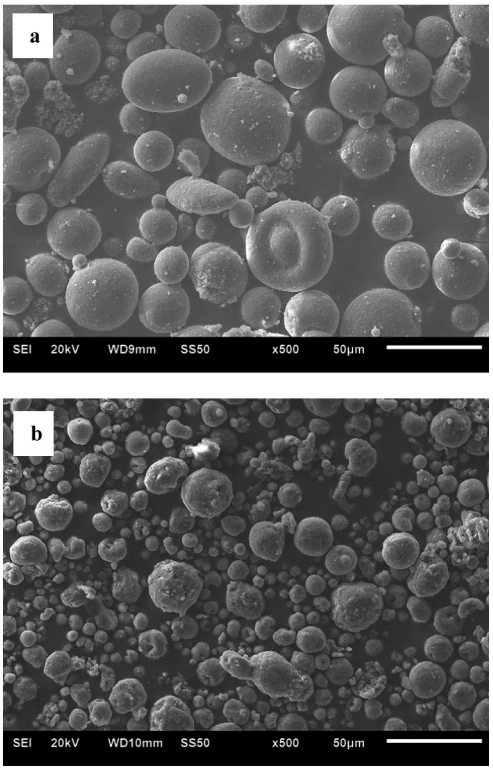


**Fig. 1. SEM micrographs of the coarse $Al_2O_3$ (a) and $Al_2O_3$ + 40 wt.% $TiO_2$ (b) coarse powders**

Rys. 1. Morfologia proszku $Al_2O_3$ (a) oraz $Al_2O_3$ + 40 wag.% $TiO_2$ (b), SEM

## METHODOLOGY

Metco 6103 and Metco 131VF (Oerlikon Metco, Germany), a commercially available powders of appropriately $Al_2O_3$ and $Al_2O_3$ + 40 wt.% $TiO_2$, with spheroidal morphology, were used in the presented study. In the article, $Al_2O_3$ powders will be described as AT0, whilst $Al_2O_3$ + 40 wt.% $TiO_2$ as AT40. The volume-surface diameters of the coarse powders were equal to AT0 powder as delivered in an agglomerated and sintered state, whilst AT40 – only in agglomerated condition. The morphologies of the powders is shown in **Fig. 1**.

Plasma spraying was carried out using SG-100 (Praxair, USA) one anode-one cathode torch, mounted on 6-axis Fanuc 2000 IA robot. The used gases were Ar and $H_2$, in the composition of 45 slpm and 5.5 slpm. The spraying paramters are given in **Table 1**. The spraying variables were spraying distance and torch scan speed.

The process parameters were selected in such a way as to distinguish the amount of heat input. Determination of this value is described in detail in **[L. 13]**. For a set of parameters defined as „1" (**Table 1**) the amount of heat was 0.53 MW/m$^2$, while for the „2" and „3" sets, it was 0.29 MW/m$^2$ and 0.19 MW/m$^2$, respectively.

Before spraying, the powders were heated to the temperature of 120°C within 2 hours, in order to avoid clogging the nozzle. Powders were injected radially and their feed rates were about 18 g/min. X5CrNi18-10 **[L. 14]** stainless steel substrates (25 mm diameter and 2 mm thickness) were cleaned with ethanol and sand blasted using corundum grit (425–500 µm, F40 **[L. 15]**) before the deposition.

The choice of substrate for plasma spraying was associated with the fact that austenitic stainless steel quite commonly used for the production of small and medium-sized components in the textile, paper, printing industries, etc. They show good resistance to chemicals that are used in the said production, while they are also exposed to increased abrasive wear. However, it seems advisable to carry out similar tests using steel grades with higher hardness to observe the effect of the substrate on the wear processes of hard coatings, in the type of $Al_2O_3$ coatings.

**Table 1. Sample code and process parameters**

Tabela 1. Oznaczenia próbek i parametry procesu

| Sample code | Spray distance, mm | Torch velocity, mm/s | Electric power, kW |
|---|---|---|---|
| AT0-1 | 80 | 300 | 35 |
| AT40-1 | | | |
| AT0-2 | 90 | 400 | |
| AT40-2 | | | |
| AT0-3 | 100 | 500 | |
| AT40-3 | | | |

The microscopic observations of powders were carried out with the use of a JEOL JSM-6610A (JEOL, Japan) microscope. The coatings' surfaces and cross sections, after metallographic preparation, were studied using scanning electron microscope PHENOM G2 PRO (Phenom-World BV, The Netherlands). To assess the porosity of coatings, images were analysed in ImageJ software, according to the ASTM Standard **[L. 16]**. The results were averaged and their standard deviation was determined. Porosity was estimated based on images taken at 1000x magnification (the average taken from 20 images), whilst the thickness of the coatings were based on the images taken at 500x magnification (the average taken from 5 measurements).

The roughness of the coatings was measured by profilometer MarSurf PS10 (Mahr, Germany). Ra, Rz, and Rt parameters were measured for the coatings in the as-sprayed condition and after the preparation for ball-on disc investigations. According to the ASTM Standard **[L. 17]**, a surface roughness Ra of 0.8 μm (or lower) is usually recommended. Therefore, coatings were surface ground before wear tests and their roughness was controlled during this process. For each coating, 5 measurements were carried out and averages and standard deviations were determined.

The microhardness of the coatings was measured with a Vickers penetrator under the load of 1.96 N (HV0.2) on the Sinowon HV-1000 apparatus (Sinowon Innovation Metrology, China), according to the standard **[L. 18]**. Ten imprints in random places of the coating were made for each sample. After measurements, the average values and standard deviations were calculated.

Adhesion of the coatings was determined in pull-off test according to the standard **[L. 19]**. The samples were glued with Distal Classic glue, of average strength 50 MPa.

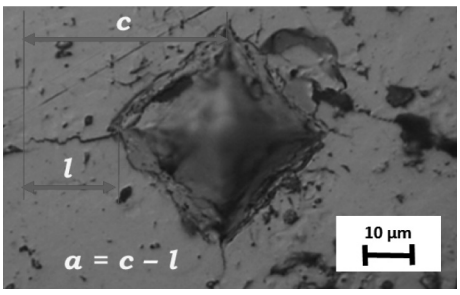


**Fig. 2. Exemplary Vickers indent in AT40 coating**
Rys. 2. Przykładowy odcisk Vickersa w powłoce AT40

Fracture toughness *Kc* was determined according to the standard **[L. 20]**. This parameter is important for the assessment of mechanical properties of ceramics **[L. 21]**. The measurements were carried out on the cross-section of the coating. Determination of *Kc* was based on measurements of cracks length, which occurred after Vickers penetration. The type of cracks is dependent on material and applied load. Two types are usually distinguished: (i) Palmqvist's – for lower loads and (ii) radial – for higher loads **[L. 23]**. The most frequently used method of crack identification is a ratio between crack length *l* and half of the diagonal length *a* (**Fig. 2**).

For *l*/*a* ratio values from 0.1 to 1.5, Niihara model is used **[L. 21**, **24]**:

$$K_C = 0.018 \cdot H^{0.6} \cdot E^{0.4} \cdot 2 \cdot a \cdot l^{-0.5} \quad \left[ MPa \cdot m^{-\frac{1}{2}} \right] \tag{1}$$

where
*Kc* – fracture toughness resistance ,
*H* – Vickers hardness [MPa],
*E* – fracture toughness resistance [MPa],
2*a* – imprint diagonal [m],
*l* – average length of cracks [m].

When the *l*/*a* ratio value is more than 1.5, an Anstis model is used **[L. 21**, **25]**:

$$K_C = 0.016 \cdot \left( \frac{E}{H} \right)^{0.5} \cdot \frac{P}{c^{1.5}} \quad \left[ MPa \cdot m^{-\frac{1}{2}} \right] \tag{2}$$

where
*Kc* – fracture toughness resistance ,
*E* – fracture toughness resistance [MPa],
*H* – Vickers hardness [MPa],
$c = a + l$ – total length of crack [m],
*P* – maximum load of penetrant [N].

Based on the results of morphology, the microstructure and mechanical properties of the coatings obtained for various spraying parameters, the optimal deposition conditions were chosen. Next, AT0 and AT40 were sprayed and tested for their wear resistance.

Tribological tests were carried out with using of ball-on-disc T-11 tribometer (Rtec instruments, USA) in technically dry friction conditions, according to the ASTM G99 standard **[L. 14]**. As a counter-part, 6 mm diameter 100Cr6 bearing steel balls were used (Ra = 0.025 μm, 60–66 HRC). Sliding was performed under ambient conditions over of period of 500 m at a sliding velocity of 0.1 m/s and a normal load of 5 N. Four replicate wear tests were carried out and the average results were reported. The worn surface of the coatings were observed on a scanning electron microscope (SEM) Phenom G2 PRO. Traces of wear were determined using a contact profilometer (Surtronic 25, Taylor Hobson) and the volumetric wear of the tested coatings was determined by the length of friction path and applied load.

## RESULTS AND DISCUSSION

The morphology of the manufactured AT0 and AT40 coatings are presented in **Fig. 3** and **Fig. 4**. Although all

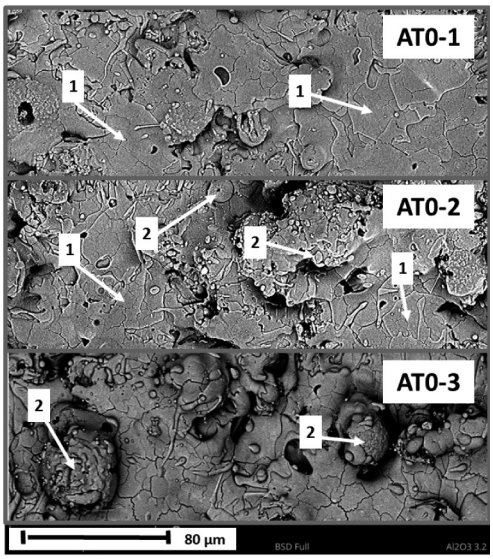


**Fig. 3. Morphology of AT0 coatings: 1 – well melted lamellas, 2 – non-melted powder particles**

Rys. 3. Morfologia powłok AT0: 1 – obszary przetopionego proszku, 2 – obszary z fragmentami niestopionych proszków

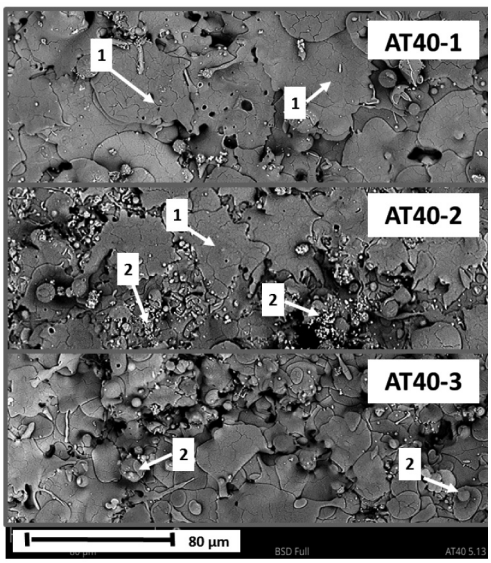


**Fig. 4. Morphology of AT40 coatings: 1 – well melted lamellas, 2 – non-melted powder particles**

Rys. 4. Morfologia powłok AT40: 1 – obszary przetopionego proszku, 2 – obszary z fragmentami niestopionych proszków

coatings are of lamellar structure, which is representative for plasma spraying, the influence of spraying parameters on the quality of obtained coatings is very visible. Both in the case of AT0 and AT40 coatings, the hottest spraying parameters result in the presence of fully melted particles, observed in the form of splats (**Fig. 3a** and **Fig. 4a**). Increased spraying distance and torch scan speed, led to the presence of non-melted powder particles, both for AT0 and AT40 powder (**Fig. 3b** and **Fig. 4b)**, especially noticeable in the case of the longest spraying distance and the fastest speed of the torch (**Fig. 3c** and **Fig. 4c**). Similar relationships were observed in work **[L. 26]**, where it was found that increasing the spraying distance enhances solidification of the molten particles. If the particles are solidified before their impact on the substrate surface, they may bounce away without forming the coating, hence the coating efficiency will decrease.

The microstructures of the manufactured coatings (presented in **Fig. 5** and **Fig. 6**, of 160–200 µm thicknesses) show, similarly as in the case of topography, the interdependences of the spraying parameters. All cross sections have a typical structure of thermally sprayed coatings, with some cracks, voids, and porosity **[L. 27**, **28]**; however, their intensity is different. Coatings sprayed in the hottest conditions, AT0-1 and AT40-1 (**Fig. 6a** and **Fig. 6a**), are of the lower porosity (**Fig. 7** and **Fig. 8**). Coatings AT0-2 and AT40-2 (**Fig. 6b** and **Fig. 6b**) are more porous, but they are still well bonded with the substrate, contrary to the AT40-3 coating (**Fig. 6c**), which together with AT0-3 coating (**Fig. 6c**) is of the highest porosity. The porosity of coatings seemed to be repeatable as the standard deviation based on 20 micrographs was in the range of 1–2%.

The results of coatings microhardness and values of porosity are presented in Figs. 7 and 8. When comparing the coatings, AT0–1/AT0–2/AT0–3, as well as: AT401/AT40–2/AT40–3, it could be seen that the microhardnesses reach similar values, notwithstanding the used spraying parameters. The differences in these values were so negligible that optimal spraying conditions were considered those that resulted in a favorable compromise between microhardness and low coating porosity (80 mm of spraying distance and 300 mm/s of torch scan speed). Additionally, it should be noted that all AT0 coatings are of higher hardness than AT40 coatings. It is also confirmed by literature **[L. 29]**.

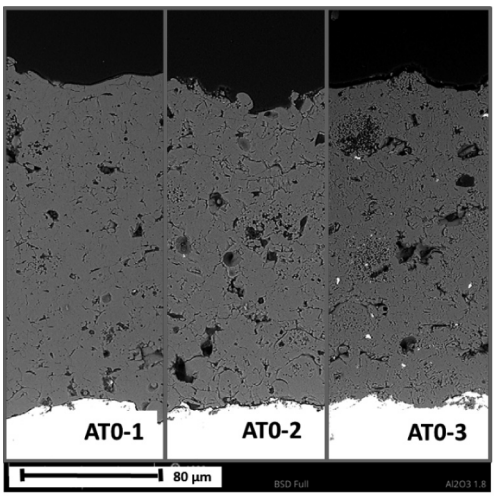


**Fig. 5. Microstructure of AT0 coatings**

Rys. 5. Mikrostruktura powłok AT0

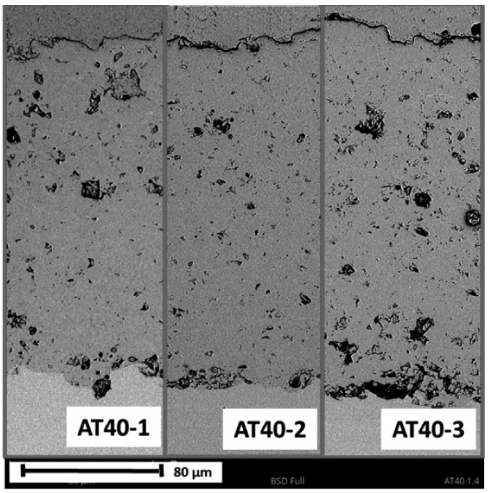


**Fig. 6. Microstructure of AT40 coatings**
Rys. 6. Mikrostruktura powłok AT40

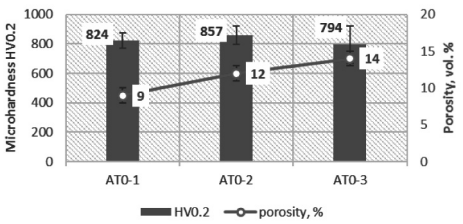


**Fig. 7. Mean microhardness (HV0.2) and porosity values of AT0 coatings**
Rys. 7. Średnie wartości mikrotwardości (HV0.2) oraz porowatości powłok AT0

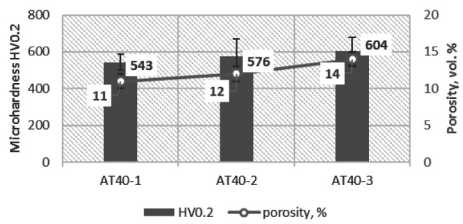


**Fig. 8. Mean microhardness (HV0.2) and porosity values of AT40 coatings**
Rys. 8. Średnie wartości mikrotwardości (HV0.2) oraz porowatości powłok AT40

The influence of spraying parameters was observed in the reference to the adhesion of coatings onto the substrate (**Fig. 9**). The highest amount of heat during spraying (for both AT0 and AT40 coatings) provides the highest adhesion of the coatings. This is probably related to the morphology and microstructure of the coatings, i.e. a greater number of defects (porosity, presence of not fully melted particles, micro-cracks) in AT0–2, AT0–3, AT40–2, AT403 coatings than in AT0–1 and AT0–2 coatings causes a decrease in the adhesion between the coatings and substrates. This is confirmed by the observations of Djendel **[L. 28]**, who also observed that increasing the spraying distance leads to a decrease in adhesion of coatings due to cooling and deceleration (and, as a result, lower kinetic energy) of particles moving in the plasma stream. It is assumed that high adhesion of the AT40–3 coating may be associated with the high porosity of the coating, because the adhesive probably penetrated the voids in the coating, which led to its strengthening and an increase in its adhesion. Nevertheless, the obtained adhesion values can be considered as satisfactory, since they are about 1.5 times higher than those obtained by Djendel **[L. 28]** for the same distance of AT3 powder spraying.

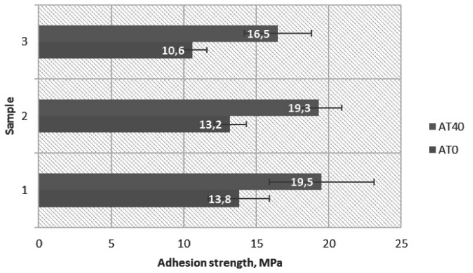


**Fig. 9. Mean adhesion strength of AT0 and AT40 coatings**
Rys. 9. Średnie wartości przyczepności powłok AT0 i AT40

In order to determine the value of fracture toughness *Kc*, 10 imprints were made in each sample under load P = 9.81 N. Then *Kc* values were calculated according to the Anstis model (**Fig. 10**). For coating systems, it is expected that the crack growth resistance increases once the splats are well melted and bonded, so the failure do not propagate, e.g., along the weak splat boundaries **[L. 30]**. This is consistent with the obtained results AT0–1 and AT40–1 coatings (with the best melted lamellas), which are of enough high fracture toughness that the values are higher than those presented in the literature (of the order of 1–2 MPa·m$^{1/2}$) **[L. 30]**.

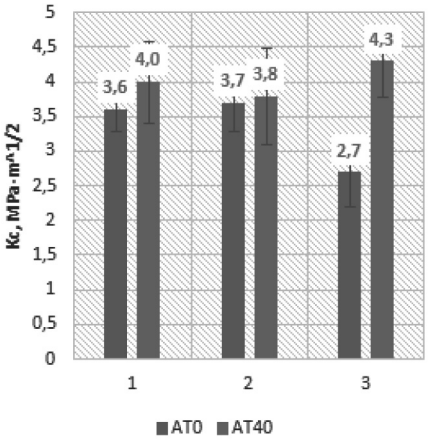


**Fig. 10. Mean values of fracture toughness *Kc* of AT0 and AT40 coatings**
Rys. 10. Średnie wartości odporności na kruche pękanie *Kc* powłok AT0 i AT40

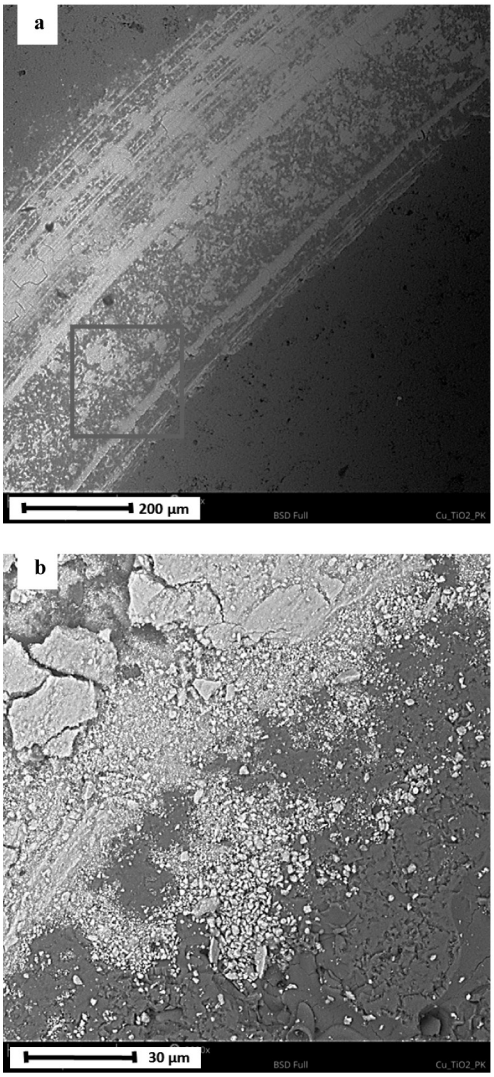


**Fig. 11. Wear tracks of AT0 coating: a – overall view, b – the detailed view of area marked in Fig. 11a**

Rys. 11. Ślady wytarcia powłoki AT0: a – widok ogólny, b – powiększenie obszaru zaznaczonego w czerwonej ramce na **Rys. 11a**

The wear resistance of coatings is not only related to properties such as microhardness and fracture resistance, but it also includes the adhesion of coatings and microstructural characteristics, such as porosity and cracks **[L. 31**, **32]**. Therefore, on the basis of morphology, microstructure and mechanical properties, AT0–1 and AT40–1 coatings were selected for further investigations of wear resistance. These coatings were found to have the most favorable combination of these properties.

The samples were surface ground to reduce the roughness Ra, according to **[L. 14]**, to 0.5 µm and 0.4 µm for AT0–1 and AT40–1 coatings, respectively (the output Ra values were 7.9 µm and 5.5 µm). The volume wear rate of coatings were equal to $1{,}03 \pm 0{,}24 \cdot 10^3$ µm/N·m (AT0–1) and $2{,}63 \pm 0{,}65 \cdot 10^3$ µm/N·m (AT40-1). As expected **[L. 33]**, $Al_2O_3$ coatings have higher hardness and, as a result, a higher wear resistance than $Al_2O_3$ + 40 wt.% $TiO_2$ coatings. The obtained results are confirmed by papers **[L. 30]** and **[L. 34]**, i.e. higher hardness results in lower wear of the coating, while higher porosity results from increased coating wear rate.

Wear tracks are shown in **Fig. 11** and **Fig. 12**. The morphology of the worn coatings and the present debris were observed. In the case of the AT0–1 coating, numerous scratches of different depths (**Fig. 11a**) as well as wear products on the working surface (**Fig. 11b**) are visible. The surface of AT40–1 coating was characterized by different morphology, indicating a greater width (**Fig. 12a**) and depth (**Fig. 12b**) of the wear race than in the case of AT0–1 coating. SEM observations are consistent with the results of tribological tests, which determine the volume wear of the coating. In both cases, adhesive and abrasive wear and the tearing of coatings is

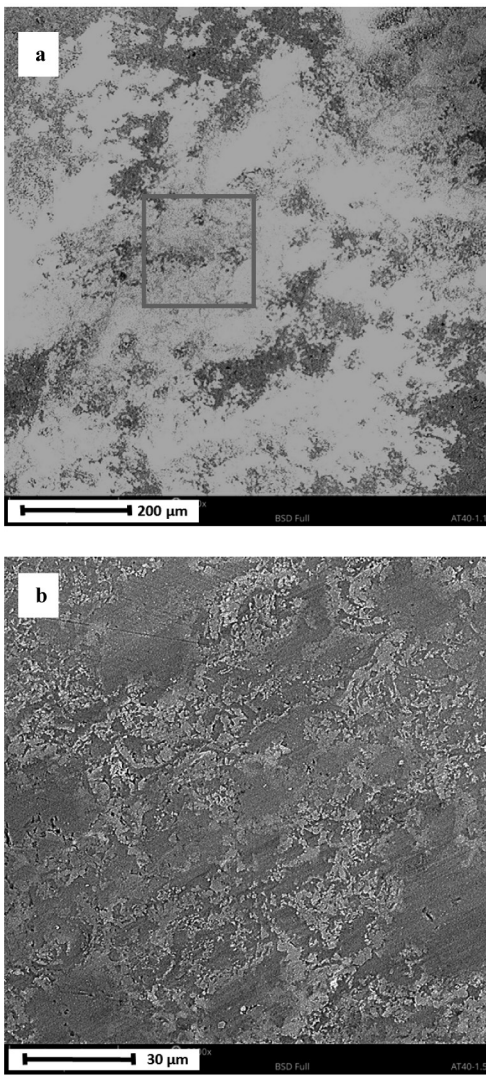


**Fig. 12. Wear tracks of AT40 coating: a – overall view, b – the detailed view of area marked in Fig. 12a**

Rys. 12. Ślady wytarcia powłoki AT40: a – widok ogólny, b – powiększenie obszaru zaznaczonego w czerwonej ramce na **Rys. 12a**

visible. The high friction coefficient obtained as a result of tests for coatings (0.59 and 0.68) indicate that the wear products observed in microscopic images may have caused the partial breakdown of the coating.

The formation and accumulation of particles that are wear products have led to a high coefficient of friction. These particles are generated in sliding contact and play a key role in determining the coefficient of friction as well as affect the friction process. These particles are usually generated in the sliding contact and play a critical role in determining friction, while their effects depend on their chemical composition and mechanical properties. In the current study, the particles were generated from hard $TiO_2$ and $Al_2O_3$ debris, which could significantly increase the coefficient of friction and accelerate the wear of the coatings. Loose wear debris must agglomerate to form larger particles that, when combined with other large particles produced directly from the wear coating, caused the quantity and size of entrapped wear particles to exceed a critical value. The wear process then went into severe abrasive wear stage, where the strong dynamic coupling between friction and abrasive wear took place, i.e. the friction coefficient increased significantly because of the increasing quantity of entrapped particles. On the other hand, the increased coefficient of friction resulted in higher shear stresses, which in turn accelerated the wear and the breakdown of the coating. The friction coefficient reached the values of 0.59 and 0.68, which are close to the typical contact between the substrate material and the ball used for testing. In the meanwhile, the friction between the ball and the austenitic stainless

had to reach its maximum because the coating was damaged, and many wear particles were formed on the surface of the coating, and these entrapped wear particles can lead to separation of the contact surface. The amount of wear particles will affect the actual contact surface as well as the depth of the penetration of each wear particle. The coefficient of friction is not a material property that can be affected by many factors. The coating's friction coefficient depends primarily on four important factors; coating hardness, coating thickness, surface roughness, and trapped dirt. In current research, this may be due to the entrapment of large wear particles and the partial disintegration of the coating. However, the accumulation and entrapment of large wear particles initiated the increasing quantity (density) and the enlarged size of the wear particles, which resulted in friction due to hard particles and led to a rapid increase in the friction coefficient.

## SUMMARY

In the article, APS sprayed coatings of $Al_2O_3$ and $Al_2O_3$ + 40 wt.% $TiO_2$ were investigated. All coatings were successfully applied on a steel substrate. The best process parameters allowed the obtaining of coatings with well-melted particles and high microhardness, low porosity, and good adhesion. These coatings were characterized by good fracture toughness and thus resistance to initiation and propagation of cracks, which is important in the selection of coatings for wear tests. Ball-on-disc tests proved that $Al_2O_3$-based coatings (with a higher microhardness and lower porosity) show a lower degree of wear than $Al_2O_3$ + 40 wt.% $TiO_2$. (TiO2 has lower microhardness and higher porosity). The coatings were worn, but there were also surface cracks. Loose, crushed fragments of the coating present in the contact zone intensified micro-cutting, which led to abrasive wear. The wear particles of $TiO_2$ and $Al_2O_3$ coating played a very important role in friction and wear processes. The initiation of wear particle flow marks the start of a stage with high friction, which directly affected the wear life of the coatings. In future studies, further friction and wear experiments of different hard coatings will be performed in order to describe the estimation of wear life of hard coatings.

## REFERENCES

1. Berger L.M., Sempf K., Sohn Y.J., Vassen R.: Influence of Feedstock Powder Modification by Heat Treatments on the Properties of APS-Sprayed $Al_2O_3$-40% $TiO_2$ Coatings, Journal of Thermal Spray Technology, 27, 2018, pp. 654–666.
2. Vardelle A. i in.: The 2016 Thermal Spray Roadmap, Journal of Thermal Spray Technology, 25, 8 (2018), pp. 1376––1440.
3. Global Thermal Spray Market – Segmented by Product Type, By End-User Industry, and Geography – Trends and Forecasts (2015–2020), (2016), Growth Report Analysis, Mordor Intelligence.
4. Toma F.L., Berger L.-M., Stahr C.C., Naumann T., Langner S.: Microstructures and Functional Properties of Suspension-Sprayed $Al_2O_3$ and $TiO_2$ Coatings: An Overview, Journal of Thermal Spray Technology, 19, 1–2 (2010), pp. 262–274.

5. Góral A., Żórawski W.: Charakterystyka mikrostruktury powłok Ni-$Al_2O_3$ natryskanych zimnym gazem, Przegląd Spawalnictwa, 87, 9 (2015), pp. 34–37.
6. Maruszczyk A., Dudek A., Szala M.: Research into morphology and properties of $TiO_2$ – NiAl atmospheric plasma sprayed coating, Advances in Science and Technology Research Journal, 11, 3 (2017), pp. 204–210.
7. Vargas F., Ageorges H., Fournier P., Fauchais P., López M.E.: Mechanical and tribological performance of $Al_2O_3$–$TiO_2$ coatings elaborated by flame and plasma spraying, Surface and Coatings Technology, 205, 4 (2010), pp. 1132––1136.
8. Jordan E.H., Gell M., Sohn Y.H., Goberman D., Shaw L., Jiang S., Wang M., Xiao T.D., Wang Y., Strutt P.: Fabrication and evaluation of plasma sprayed nanostructured alumina–titania coatings with superior properties, Materials Science and Engineering: A, 301, 1 (2001), pp. 80–89.
9. Di Girolamo G., Serra E.: Anti-Abrasive Nanocoatings: Current and Future Applications, 20 – Thermally sprayed nanostructured coatings for anti-wear and TBC applications: State-of-the-art and future perspectives, Woodhead Publishing, UK, Cambridge, 2015.
10. Sert Y., Toplan N.: Tribological behavior of a plasma-sprayed $Al_2O_3$-$TiO_2$-$Cr_2O_3$ coating, Materials and Technology, 47, 2 (2013), pp. 181–183.
11. Zavareh M.A., Sarhan A.A.D.M., Razak B.B.A., Basirun W.J.: Plasma thermal spray of ceramic oxide coating on carbon steel with enhanced wear and corrosion resistance for oil and gas applications, Ceramics International, 40, 9 (2014), pp. 14267–14277.
12. Bannier E., Vicent M., Rayón E., Benavente R., Salvador M.D., Sánchez E.: Effect of $TiO_2$ addition on the microstructure and nanomechanical properties of $Al_2O_3$ Suspension Plasma Sprayed coatings, Applied Surface Science, 316, 15 (2014), pp. 141–146.
13. Łatka L., Goryachev S.B., Kozerski S., Pawłowski L.: Sintering of fine particles in suspension plasma sprayed coatings, Materials, 3 (2010), pp. 3845–3866.
14. PN-EN ISO 10088-1:2014-12: Stale odporne na korozję – Część 1: Wykaz stali odpornych na korozję, 2014.
15. FEPA-Standard 42-1:2006: Grains of fused aluminium oxide, silicon carbide and other abrasive materials for bonded abrasives and for general industrial applications Macrogrits F 4 to F 220, 2006.
16. ASTM E2109-01(2014) Standard Test Methods for Determining Area Percentage Porosity in Thermal Sprayed Coatings, ASTM International, West Conshohocken, PA, 2014.
17. ASTM G99-17 (2017) Standard Test Method for Wear Testing with a Pin-on-Disk Apparatus, ASTM International, West Conshohocken, PA, 2017.
18. PN-EN ISO 4516:2004, Powłoki metalowe i inne nieorganiczne – Badania mikrotwardości metodą Vickersa i Knoopa, 2004.
19. PN-EN ISO 14916:2017-05 – Natryskiwanie cieplne – Określanie przyczepności metodą odrywania, 2017.
20. PN-EN ISO 14577-4:2017-02 – Metale – Instrumentalna próba wciskania wgłębnika do określania twardości i innych własności materiałów – Część 4: Metoda badania metalowych i niemetalowych powłok, 2017.
21. Pędzich Z., Piekarczyk J., Stobieralski L., Szutkowska M., Walat E.: Twardość Vickersa i odporność na kruche pękanie wybranych kompozytów ceramicznych, Kompozyty, 3, 2003, pp. 296–300.
22. Palmqvist S.: Occurrence of crack formation during Vickers indentation as a measure of the toughness of hard metals, Archiv für das Eisenhüttenwesen, 33, 1962, pp. 629–633.
23. Munz D., Felt T.: Ceramics: mechanical properties, failure behaviour, materials selection, Springer, US, New York 1999.
24. Niihara K.: A fracture mechanics analysis of indentation-induced Palmqvist crack in ceramics, Journal of Materials Science Letters, 2, 1983, pp. 221–223.
25. Anstis G.R., Chantikul P., Lawn B.R., Marshall D.B.: A critical evaluation of indentation techniques for measuring fracture toughness: I, Direct crack measurements, Journal of the American Ceramic Society, 64, 1981, pp. 533–538.
26. Vijay M., Selvarajan V., Yugeswaran S., Ananthapadmanabhan P.V., Sreekumar K.P.: Effect of Spraying Parameters on Deposition Efficiency and Wear Behavior of Plasma Sprayed Alumina-Titania Composite Coatings, Plasma Science and Technology, 11, 6 (2009), pp. 666–673.
27. Łatka L., Niemiec A., Michalak M., Sokołowski P.: Tribological properties of $Al_2O_3$ + $TiO_2$ coatings manufactured by plasma spraying, Tribology, 283, 1 (2019), pp. 19–24.
28. Djendel M., Allaoui O., Boubaaya R.: Characterization of Alumina-Titania Coatings Produced by Atmospheric Plasma Spraying on 304 SS Steel, Acta Physica Polonica A, 132, 3 (2017), pp. 538–540.

29. Bolelli G., Cannillo V., Lusvarghi L., Manfredini T.: Wear behaviour of thermally sprayed ceramic oxide coatings, Wear, 261 (2006), pp. 1298–1315.
30. Ghazali M.J., Forghani S.M., Hassanuddin N., Muchtar A., Daud A.R.: Comparative wear study of plasma sprayed $TiO_2$ and $Al_2O_3$-$TiO_2$ on mild steel, Tribology International, 93 (2016), pp. 681–686.
31. Wang Y., Jiang S., Wang M., Wang S., Xiao T., Strutt P.: Abrasive wear characteristics of plasma sprayed nanostructured alumina/titania coatings, Wear, 237 (2000), pp. 176–185.
32. Normand B., Fervel V., Coddet C., Nikitine V.: Tribological properties of plasma sprayed alumina-titania coatings: role and control of the microstructure, Surface and Coatings Technology, 123 (2000), pp. 278–287.
33. Sahab A.R.M., Saad N.H., Kasolang S., Saedon J.: Impact of Plasma Spray Variables Parameters on Mechanical and Wear Behaviour of Plasma Sprayed $Al_2O_3$ 3%wt $TiO_2$ Coating in Abrasion and Erosion Application, Procedia Engineering, 41 (2012), pp. 1689–1695.
34. Liu Y., Fischer T., Dent A.: Comparison of HVOF and plasma-sprayed alumina/titania coatings – microstructure, mechanical properties and abrasion behavior, Surface and Coatings Technology, 167 (2003), pp. 68–76.